Critical Strengths for Slip Events in Nanocrystalline Metals: Predictions of Quantized Crystal Plasticity Simulations

LIN LI, MYOUNG-GYU LEE, and PETER M. ANDERSON

This article studies how the monotonic and cyclic stress-strain response of nanocrystalline (NC) metals is affected by the grain-to-grain distribution of critical strengths (τ_c) for slip events, as well as plastic predeformation ($\varepsilon^p_{\text{pre}}$). This is accomplished *via* finite element simulations that capture large jumps in plastic strain from dislocation slip events—a process referred to as quantized crystal plasticity (QCP).[1] The QCP simulations show that τ_c and $\varepsilon^p_{\text{pre}}$ significantly alter the monotonic and cyclic response at small strain, but only τ_c affects the response at large strain. These features are exploited to systematically infer the τ_c and $\varepsilon^p_{\text{pre}}$ characteristics that best fit experimental data for electrodeposited (ED) NC Ni. Key outcomes are the following: (1) the τ_c distribution is truncated, with an abrupt onset of slip events at a critical stress; (2) $\varepsilon^p_{\text{pre}} = -0.4$ pct, signifying precompression; (3) there is reverse slip bias, meaning that reverse slip events are easier than forward events; and (4) highly inhomogeneous residual stress states can be enhanced or reduced by tensile deformation, depending on $\varepsilon^p_{\text{pre}}$.

DOI: 10.1007/s11661-010-0392-2

I. INTRODUCTION

A quantized crystal plasticity (QCP) model has been shown to qualitatively reproduce several distinct features of nanocrystalline (NC) metals, including *enhanced flow stress*, an *extended elasto-plastic transition strain*, and a *propensity for strain localization*.[1] The model is motivated by molecular dynamics simulations[2] that show dramatic jumps in grain-averaged plastic strain and violent oscillations in local stress due to discrete slip events. Prior application of the QCP model suggests that an asymmetric *grain-to-grain* variation in the critical resolved shear stress τ_c is consistent with these unique stress-strain features.

NC metals exhibit other distinctive mechanical features compared to their coarse-grained counterparts.[3,4] Recent reports for NC Al and Au thin films show that more than 40 pct of plastic deformation is recoverable upon unloading.[5,6] The extraordinary plastic recovery in NC metals is attributed to large residual stress, which is enhanced in principal by the quantized nature of slip and a typically large variation in microstructure, *e.g.*, grain size.[7]

Moreover, *in-situ* X-ray diffraction studies reveal that peak broadening observed during room temperature deformation of electrodeposited (ED) NC Ni is fully reversible upon unloading.[8–10] Thus, the inhomogeneous strain induced during deformation appears to be recoverable, suggesting that no permanent dislocation network forms during deformation. Also, strain-dip testing of such samples shows larger values (~GPa) for effective and internal stress compared to coarse-grained metals (~MPa).[11] These tests also reveal negative creep, which is interpreted in terms of dislocation interaction with GB ledges.[11]

Underlying deformation mechanisms in NC metals have been studied in detail using MD simulations.[12–16] The observations show formation of dislocation loops from GBs. Initially, they exist in an *incipient* state in which grain boundary pinning prevents expansion. Ultimately, they can unpin, expand through a relatively clean grain interior, and absorb into the opposite GB. As grain size decreases, the stress to unpin tends to increase and interactions between dislocations and GBs can become more important. Such a description suggests that as grain size decreases, stress states can become more inhomogeneous and strain relaxation processes may depend on the kinetics of unpinning.[5–7,10,11]

The present work incorporates *reverse slip* into QCP simulations.[1] This enables investigation of the combined effects of plastic predeformation ($\varepsilon^p_{\text{pre}}$), grain-to-grain distribution of critical strengths (τ_c), and bias (τ_{bias}) in the critical shear stress for forward *vs* reverse slip. A premise is that these quantities can be determined *via* calibration of the QCP simulations to experimental $\sigma-\varepsilon$ data. An outcome is that both monotonic and cyclic $\sigma-\varepsilon$ data are needed to determine $\varepsilon^p_{\text{pre}}$, τ_c, and τ_{bias}. For ED NC Ni (30 nm), τ_c is described best by an asymmetric distribution, a noticeable τ_{bias} exists at small plastic strain, and a residual stress state exists prior to loading. The calibrated QCP model predicts enhanced plastic recovery upon unloading, due to a very heterogeneous stress state. In special cases, deformation is observed to reduce the residual stress state, as suggested by recent X-ray diffraction studies.[10]

LIN LI, PhD Student, and PETER M. ANDERSON, Professor, are with the Department of Materials Science and Engineering, The Ohio State University, Columbus, OH 43210. Contact e-mail: Anderson.1@osu.edu MYOUNG-GYU LEE, Assistant Professor, is with the Graduate Institute of Ferrous Technology, Pohang University of Science and Technology, Pohang, Gyeongbuk 790-784, Korea.
Manuscript submitted March 21, 2010.
Article published online September 8, 2010

II. A FINITE ELEMENT/QCP MODEL

A. *FEM Representation and Boundary Conditions*

A polycrystal is modeled by a 10 × 10 × 10 array of three-dimensional brick finite elements (C3D8) using ABAQUS software.[17] The eight integration points in an element are assigned the same initial crystallographic orientation as to represent one fcc grain. Figure 1 shows an FEM sample, with each grain shaded according to the maximum Schmid factor $S_{z,\max}$ among the 12 competing ½<110>/{111} slip systems. Uniaxial loading and unloading is imposed *via* a macroscopic strain rate ($\dot{\varepsilon}_{\text{global}} = \pm 10^{-3}$/s) along the z direction, with free surface boundary conditions on the $\pm x$ and $\pm y$ faces (Figure 1).

B. *QCP Constitutive Relation*

This work employs the QCP constitutive relation introduced in Reference 1 and extends it to include reverse slip during cyclic loading. Table I summarizes the relevant notation. The nature of the QCP model is that on a grain-average scale, the plastic shear strain produced by an event on some slip system (α) with slip plane normal n and slip direction s is

$$\gamma_{ns}^{p(\alpha)} = q\gamma_{\text{target}} \qquad [1]$$

The coefficient q takes on integer values and $\gamma_{\text{target}} \propto 1/(\text{grain size})$. A *forward* event increases the magnitude of q and is activated when the resolved shear stress satisfies $\tau_{ns}^{(\alpha)} \cdot \text{sign}(\gamma_{ns}^{p(\alpha)}) \geq \tau_c$. Likewise, a *backward* event decreases the magnitude of q and is activated when $\tau_{ns}^{(\alpha)} \cdot \text{sign}(\gamma_{ns}^{p(\alpha)}) \leq -\tau_{c,b}$. The critical stress for forward *vs* backward events may differ by an amount $\tau_{\text{bias}} = \tau_c - \tau_{c,b}$. Upon activation, the plastic strain increments at a rate $\dot{\gamma}_0$ until q reaches an integer value, even if the activation condition is not satisfied continuously during the process, due to stress redistribution. Equation [1] and the activation conditions are implemented numerically, *via* an extension to conventional rate-dependent crystal plasticity theory[18] (Reference 1).

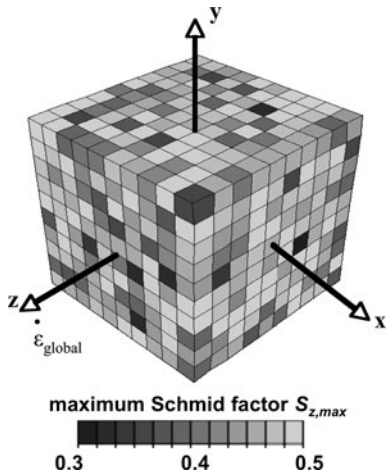

Fig. 1—Finite element model of a polycrystal with a 10 × 10 × 10 array of grains, each represented by an 8-node brick element. Uniaxial loading is applied along the z direction. Shading of each grain indicates the maximum Schmid factor among the 12 fcc slip systems in that grain.

C. *Material and Computational Parameters*

The material parameters are consistent with local elastic behavior governed by anisotropic elastic constants C_{11}, C_{12}, and C_{44} = 246.5, 147.3, and 124.7 GPa, respectively,[19] and random grain orientations consistent with an untextured polycrystal, as in Reference 1. Two distributions are considered for the nonuniform grain-to-grain values of τ_c: an asymmetric distribution described by a Gamma function (Eq. [5a], Table II) and a normal distribution (Eq. [5b], Table II). Each of these has two free parameters that control $\tau_{c,\text{mean}}$ and $\tau_{c,\min}$. In general, the most severe slip events are modeled by selecting $\gamma_{\text{target}} = \min(1.2\ \mathbf{b}/d,\ \tau_c/60\ \text{GPa})$, where the Burgers vector magnitude $\mathbf{b}$ = 0.25 nm and a uniform grain size d = 30 or 50 nm is applied. The first expression for γ_{target} corresponds to slip of a cubic grain of edge length d on a glide plane through the center. The second expression is an estimate of the largest γ_{target} that can be accommodated without reversing the sign of $\tau_{ns}^{(\alpha)}$ during expansion of the loop across the grain. This is termed the *positive driving force* condition.[1] The first expression normally applies, but there is typically a subset of ~15 pct grains with smaller τ_c values for which the second expression applies. In addition, a variety of τ_{bias} values are considered.

The primary computational parameters are the local strain rate $\dot{\gamma}_0 = 2 \cdot 10^{-2}$/s contributed by an active slip system and the macroscopic strain rate $\dot{\varepsilon}_{\text{global}} = 1 \cdot 10^{-3}$/s. The former is an order of magnitude larger so that deformation due to local slip is viewed as relatively instantaneous compared to macroscopic deformation. A maximum time increment $\Delta t = 2 \cdot 10^{-2}$ s is specified to ensure that a quantized slip event is captured in several time-steps. Prior studies[1] demonstrate that a 1000 grain model is sufficiently large so that the macro $\sigma-\varepsilon$ response is independent of the number of grains. A typical analysis with 1000 grains for 100 time-steps requires ~4.5 CPU hours with the Glenn system at the Ohio Supper Computer Center.[20]

Table I. Summary of Notation

$\dot{\varepsilon}_{\text{global}}$	macroscopic strain rate along z-axis
σ_{global}	macroscopic stress along z-axis
σ_0	macroscopic stress for onset of the first slip event
$\tau_{ns}^{(\alpha)}$	local resolved shear stress, slip system α
$\gamma_{ns}^{p(\alpha)}$	local plastic shear strain, slip system α
γ_{target}	local shear strain produced by a slip event
$\dot{\gamma}_0$	local plastic shear strain rate during a slip event
τ_c	local critical resolved shear stress for a forward slip event
$\tau_{c,b}$	local critical resolved shear stress for a backward slip event
τ_{bias}	$\tau_c - \tau_{c,b}$
τ_c^{eff}	minimum additional τ_{ns} to initiate a slip event
$\Delta\tau$	jump in local resolved shear due to a slip event
$\varepsilon_{\text{pre}}^p$	uniaxial plastic prestrain along z-axis prior to tensile testing

Table II. Multistep Process to Calibrate QCP Simulations to Experimental Data

Step	Quantity	Method to Calculate
1	$\Delta\tau$	$\Delta\tau = -c_1 Mb/d,\ c_1 = 1.44,\ M = \mu(7-5\nu)/[15(1-\nu)]$ [2]
2a	$\tau_{c,\text{mean}}$	$(\tau_c - 0.5\lvert\Delta\tau\rvert)_{mean} \approx \bar{S}_{Z,\max}\,\sigma_{\text{plateau}},\ \bar{S}_{Z,\max} = 0.45$ [3]
2b	$\tau_{c,\min}$	$\tau_{c,\min} = \sigma_0 S_{z,\max},\ S_{z,\max} = 0.5$ [4]
3	τ_c distrib candidates	$P_a(\tau,k,\theta) = (\tau-\tau_{c,\min})^{k-1}(\Gamma(k)\theta^k)^{-1}\exp\left[-(\tau-\tau_{c,\min})/\theta\right]$ [5a] $k = 1,\ \theta = \tau_{c,\text{mean}} - \tau_{c,\min}$ $P_s(\tau,\tau_{c,\text{mean}},\sigma) = (\sigma\sqrt{2\pi})^{-1}\exp\left[-(\tau-\tau_{c,\text{mean}})/2\sigma^2\right],\ \sigma = \theta/3$ [5b]
4	γ_{target}	$\gamma_{\text{target}} = \min(c_2 b/d,\ \tau_c/c_2 M),\ c_2 = 1.2,\ M = $ (see Eq. [2]) [6]
5a	τ_c distrib $P_a(\tau,k,\theta)$	best fit to cyclic data at large strain
5b	τ_{bias}	best fit to cyclic data at large and small strain
6	$\varepsilon^p_{\text{pre}}$	best fit to tensile data at small strain

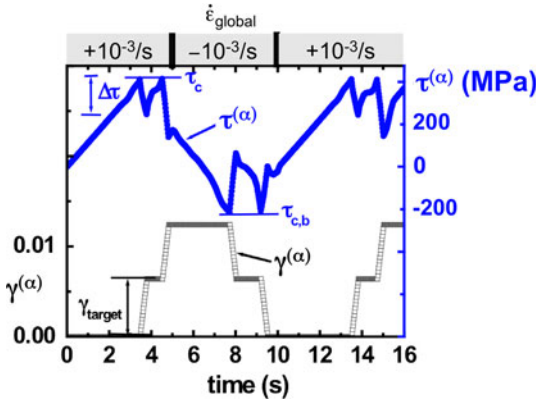

Fig. 2—Evolution of the local plastic strain $\gamma^{(\alpha)}$ and local resolved shear stress $\tau^{(\alpha)}$ on a specific slip system α in an arbitrary interior grain. The applied global strain rate reverses sign at 5 and 10 s.

Figure 2 shows the evolution of $\gamma^{p(\alpha)}_{ns}$ and $\tau^{(\alpha)}_{ns}$(MPa) *vs* time (seconds) for a specific slip system α in an interior grain with $\gamma_{\text{target}} = 6\cdot 10^{-3}$. Three periods are shown: $\dot{\varepsilon}_{\text{global}} = +10^{-3}$/s from 0 to 5 seconds; $\dot{\varepsilon}_{\text{global}} = -10^{-3}$/s from 5 to 10 seconds; and $\dot{\varepsilon}_{\text{global}} = +10^{-3}$/s from 10 to 16 seconds. During the first period, τ_c is reached twice, so that q increments from 0 to 1 and then 1 to 2. During the second period, $-\tau_{c,b}$ is reached twice, producing $q = 0$. In the third period, two forward events occur, producing $q = 2$. Thus, $\gamma^{p(\alpha)}_{ns}$ is quantized in units of γ_{target}. Note that $\tau_c = 428.4$ MPa *vs* $\tau_{c,b} = 228.4$ MPa, so that $\tau_{\text{bias}} = 200$ MPa. In Figure 2, $\tau^{(\alpha)}_{ns}$ sometimes increases in a nonlinear fashion due to stress redistribution arising from slip events in neighboring grains. About 15 time-steps (corresponding to 0.3 seconds) are required to fully implement a slip event, thereby ensuring sufficient computational resolution.

D. *Experimental Data*

The QCP predictions are compared to data for ED NC Ni from two sources. The first is monotonic tensile data by Ebrahimi *et al.*[21] on material with a mean grain size, $d_{\text{mean}} = 50$ nm (Sections III–A and B). The second is monotonic and cyclic uniaxial data by Van Swygenhoven *et al.* on material from Goodfellow[10] with $d_{\text{mean}} = 30$ nm (Sections III–C and D).

III. MODEL CALIBRATION

A. *Effect of Prestrain on σ−ε Response*

QCP simulations show that plastic predeformation ($\varepsilon^p_{\text{pre}}$) alters the macro $\sigma-\varepsilon$ response primarily at small strain (<1 pct) and less so at larger strain. Figure 3(a) shows the results for $\varepsilon^p_{\text{pre}} = -3$ pct, 0, and 3 pct, assuming an asymmetric τ_c distribution (Figure 3(b)) and $\tau_{\text{bias}} = 0$. Square symbols in Figure 3(a) are the experimental results for ED NC Ni with $d_{\text{mean}} = 50$ nm.[21] Precompression produces a "rounded," gradual approach to the plateau stress (σ_{plateau}), while pretension generates more abrupt yield. A quantitative assessment is that the width of the transition is $\Delta\varepsilon^p \sim 1.6$ pct for $\varepsilon^p_{\text{pre}} = -3$ pct *vs* 0.05 pct for $\varepsilon^p_{\text{pre}} = 3$ pct, where $\Delta\varepsilon^p$ is the plastic strain increment over which the flow stress increases from an initial value σ_0 to approximately 0.9 σ_{plateau}.

Figure 3(a) also shows that the effect of predeformation diminishes with increasing strain. All cases approach $\sigma_{\text{plateau}} = 1200$ MPa, regardless of $\varepsilon^p_{\text{pre}}$. This suggests that deformation history is "forgotten" as plastic flow develops. An important caveat, however, is that the τ_c distribution does not evolve with plastic deformation in these simulations. In reality, the τ_c distribution may change as the density and strength of grain boundary pinning sites evolve with deformation.

Predeformation can be viewed in terms of the residual stress state it induces and how this stress state biases subsequent yield. Figures 3(c) and (d) show the distribution of τ_c^{eff}, defined as the additional resolved shear stress to initiate a slip event on the most favored slip system at an integration point. Among the $\alpha = 1$ to 12 systems, the most favored one renders $\left[\tau_c - \text{sign}\left(S_Z^{(\alpha)}\right)\tau^{(\alpha)}_{ns}\right]\Big/\left|S_Z^{(\alpha)}\right|$ a minimum, where $S_Z^{(\alpha)} = (n_z \cdot s_z)^{(\alpha)}$ is the Schmid factor for tension along the z-axis. Precompression tends to spread out the τ_c^{eff} distribution, so that regions B and C in the original distribution (Figure 3(b)) shift, respectively, to regions B' and C' (Figure 3(c)). This is consistent with residual tension ($\sigma_z > 0$) for region B' and residual compression for C'. The grains in region B' readily yield as the tensile test commences because τ_c^{eff} is so small. Analytic modeling[1] demonstrates that the resulting "rounded"

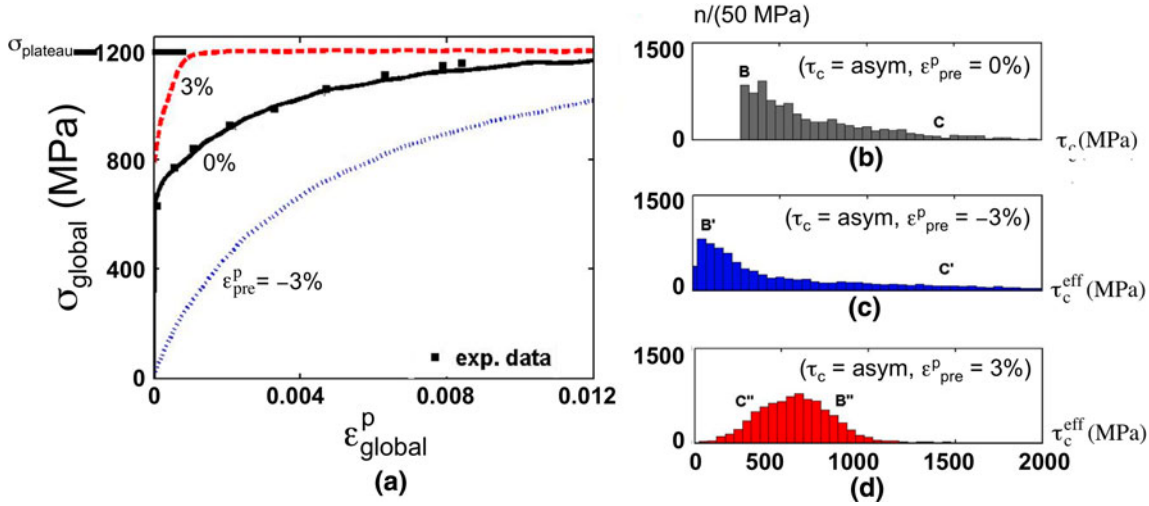

Fig. 3—(*a*) Predicted tensile stress–plastic strain response of an untextured polycrystal with τ_c = asymmetric distribution; ε^p_{pre} = −3 pct, 0, and 3 pct; and τ_{bias} = 0. Square symbols denote the experimental data for ED NC Ni with d_{mean} = 50 nm.[21] (*b*) Asymmetric distribution, (*c*) τ_c^{eff} distribution after plastic predeformation ε^p_{pre} = −3 pct, and (*d*) ε^p_{pre} = 3 pct.

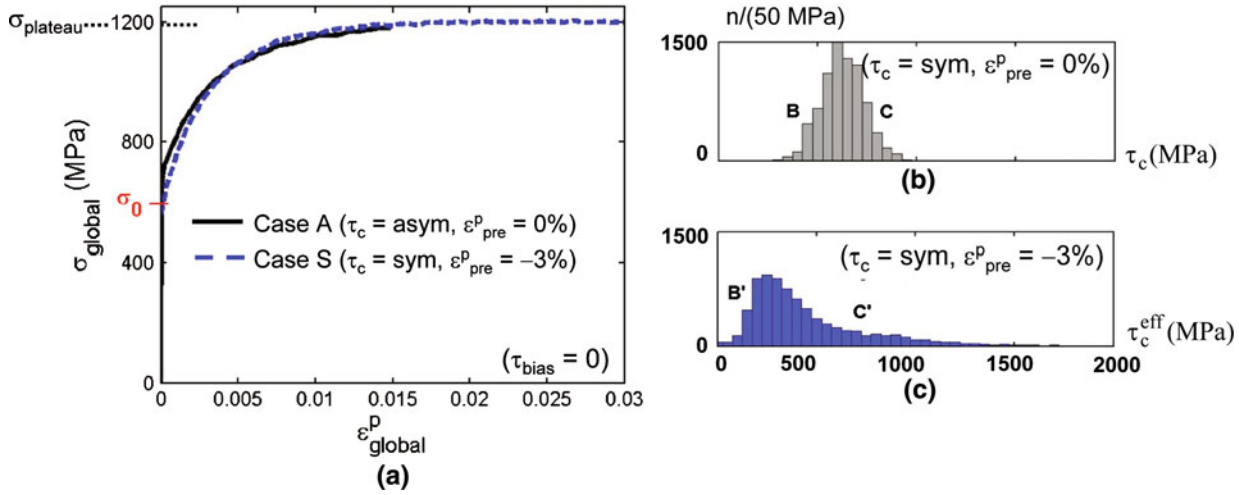

Fig. 4—(*a*) Predicted tensile stress–plastic strain response of an untextured polycrystal for case A: (τ_c,ε^p_{pre}) = (asym, 0) and case S: (τ_c, ε^p_{pre}) = (sym, −3 pct). τ_{bias} = 0. (*b*) Symmetric τ_c distribution. (*c*) τ_c^{eff} distribution after plastic predeformation ε^p_{pre} = −3 pct.

σ-ε behavior stems from the abrupt rise in the distribution at *B′* (Eq. [13][1]). Alternately, pretension produces a more symmetric τ_c^{eff} distribution (Figure 3(d)) that is associated with a less rounded σ−ε response. In particular, regions *B* and *C* in the original distribution (Figure 3(b)), respectively, shift to regions *B″* and *C″* (Figure 3(d)). Thus, precompression and pretension produce opposite shifts in regions *B* and *C* and generate very different τ_c^{eff} distributions (asymmetric *vs* symmetric).

B. *Nonuniqueness from Monotonic σ−ε Response Alone*

Similar monotonic σ−ε responses can be achieved with more than one combination of (τ_c, ε^p_{pre}). Figure 4(a) shows that the asymmetric τ_c distribution (Figure 3(b)) with ε^p_{pre} = 0 (case *A*: solid curve) and a symmetric τ_c distribution (Figure 4(b)) with ε^p_{pre} = −3 pct (case *S*: dashed curve) produce similar σ−ε responses. This observation, coupled with the discussion in Section III–A, suggests that both combinations of (τ_c, ε^p_{pre}) should produce similar τ_c^{eff} distributions. A comparison of Figures 3(b)) (case *A*) and 4(c) (case *S*) confirms similar τ_c^{eff} distributions. Thus, a unique combination (τ_c, ε^p_{pre}) cannot be deduced from monotonic σ−ε data alone.

C. *Uniqueness from Monotonic and Cyclic σ−ε Response*

Cyclic data at both large and small strain enables unique combinations of (τ_c, ε^p_{pre}) to be deduced, as well as estimates of τ_{bias}. Figure 5(a) shows the predicted σ−ε response when strained well into the plateau region ($\varepsilon^p_{global} > 2.5$ pct), and then cycled. The hysteretic $\sigma-\varepsilon^p$ response is relatively independent of ε^p_{global} and ε^p_{pre}. However, it is very dependent on the τ_c distribution and τ_{bias}. In particular, case *A* (τ_c = asymmetric, ε^p_{pre} = 0, τ_{bias} = 0) has a very pronounced hysteretic width

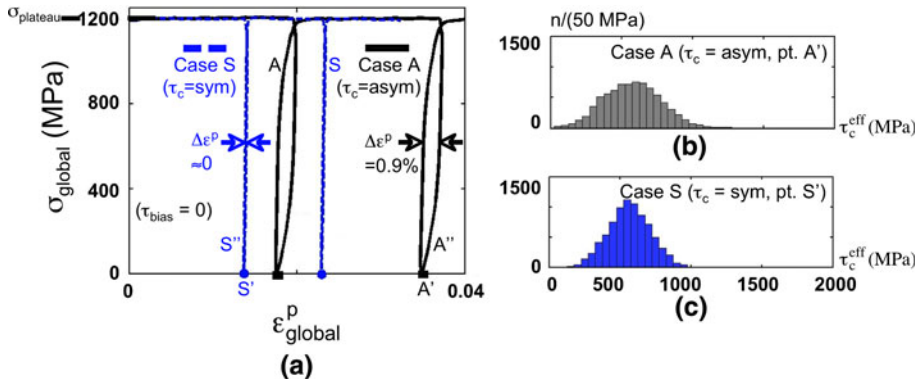

Fig. 5—(*a*) Predicted cyclic stress–plastic strain response of an untextured polycrystal at large strain, for case A (τ_c, ε^p_{pre}) = (asym, 0) and case S (τ_c, ε^p_{pre}) = (sym, −3 pct). τ_{bias} = 0. (*b*) τ_c^{eff}distribution for case A, after unloading to pt. A′. (*c*) τ_c^{eff}distribution for case S, after unloading to pt. S′.

($\Delta\varepsilon^p$ = 0.9 pct at σ = 600 MPa), while case *S* (τ_c = symmetric, ε^p_{pre} = −3 pct, τ_{bias} = 0) has negligible width ($\Delta\varepsilon^p \sim 0$).

Some insight is gained from the τ_c and τ_c^{eff} distributions. During monotonic straining along the plateau, τ is expected to reach τ_c in numerous grains, so that the τ distribution mimics the asymmetric τ_c distribution (Figure 3(b)) for case *A* and symmetric τ_c distribution (Figure 4(b)) for case *S*. Thus, the polycrystalline system reaches criticality along the plateau.[22] Upon unloading to points *A′* and *S′* in Figure 5(a), the asymmetric distribution offers a large fraction of weak (small τ_c) sites at the onset of reverse slip, and accordingly, there is a large amount of reverse slip (region *A″*, Figure 5(a)). In contrast, the symmetric distribution has a smaller fraction of weak sites and, consequently, less reverse slip (region *S″*, Figure 5(a)). Upon reloading, the τ_c^{eff} distributions (Figures 5(b) and (c)) apply. The distribution for case *A* has a larger number of sites at smaller τ_c^{eff}, so that forward slip is more pronounced compared to case *S*.

A general characteristic of the asymmetric distribution (Figure 3(b)) is that a relatively large fraction of weak (small τ_c) sites are balanced by a relatively small fraction of strong sites (Figure 3(b)). These weak sites supply large amounts of forward and backward slip events during cycling. In principle, symmetric (normal) distributions other than Figure 4(b) can be considered. However, the distributions cannot be shifted or widened arbitrarily, since the mean controls the plateau stress (Eq. [3], Table II) and the minimum controls the onset of yield and also must satisfy the *positive driving force* condition (Section II–C).

Figure 6 shows the corresponding outcomes when a smaller plastic strain ($\varepsilon^p_{global} \sim 0.3$ pct) is imposed, followed by cycling. As before, case *A* (τ_c = asymmetric, ε^p_{pre} = 0, and τ_{bias} = 0) has a larger hysteretic width ($\Delta\varepsilon^p$ = 0.02 pct at σ = 425 MPa) than case *S* (τ_c = symmetric, ε^p_{pre} = −3 pct, and τ_{bias} = 0). Compared to Figure 5(a), the hysteretic widths at this smaller strain are an order of magnitude or even smaller.

D. *Application to ED NC Ni (30 nm)*

The results in Sections III–A through III–C produce a formal, multiple-step procedure to calibrate the QCP

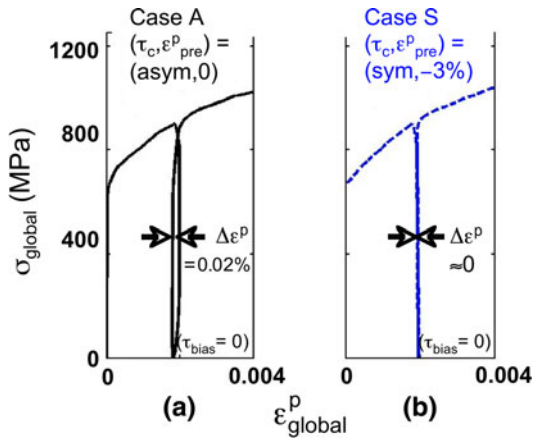

Fig. 6—(*a*) Predicted cyclic stress–plastic strain response of an untextured polycrystal at small strain, for (a) case A: (τ_c, ε^p_{pre}) = (asym, 0) and (*b*) case S: (τ_c, ε^p_{pre}) = (sym, −3 pct). τ_{bias} = 0.

simulations to monotonic and cyclic data. These steps are summarized in Table II and applied to NC Ni with a mean grain size of 30 nm.[10] The first four steps originate from prior work.[1] First, the maximum stress jump $\Delta\tau$ (Figure 2) associated with a slip event is estimated from the mean grain size d_{mean}, Burgers vector magnitude **b**, elastic shear modulus μ, and Poisson's ratio ν (Eq. [2], Table II). Second, the mean of the critical strength distribution $\tau_{c,mean}$ is estimated from the plateau stress $\sigma_{plateau}$ and the polycrystalline average of the largest Schmid factor $\bar{S}_{z,max}$ (= 0.45 for an untextured fcc polycrystal) in each grain (Eq. [3], Table II). In addition, the minimum in the critical strength distribution $\tau_{c,min}$ is estimated from the initial polycrystalline yield strength σ_0 and the global maximum Schmid factor $S_{z,max}$ (=0.5) (Eq. [4], Table II). Third, $\tau_{c,mean}$ and $\tau_{c,min}$ are used to generate two candidate τ_c distributions: an asymmetric Gamma distribution and a normal distribution (Eqs. [5a] and [5b], Table II). Fourth, the quantized jump γ_{target} for each grain is specified as discussed in Section II–C and summarized in Table II, Eq. [6].

The remaining steps 5 and 6 identify the best distribution (asymmetric or normal) and optimal values of τ_{bias} and ε^p_{pre}. Step 5 determines the best fit to cyclic

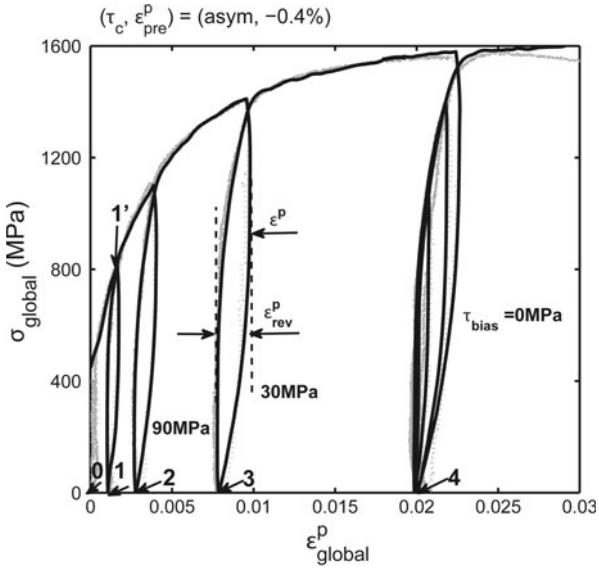

Fig. 7—Cyclic stress–plastic strain results for the best fitting QCP simulation (solid curve) *vs* experimental data (gray curve) for ED NC Ni with mean grain size d_{mean} = 30 nm. The simulation uses τ_c = asym, ε^p_{pre} = −0.4 pct. τ_{bias} = 0, 30, and 90 MPa depending on the imposed global plastic strain. Table III provides parameters.

$\sigma-\varepsilon^p$ response. Figure 7 shows the QCP results (solid curve) that best fit the experimental data (gray curve). The asymmetric τ_c distribution successfully captures the hysteretic widths and also the magnitude of reverse strain at unloading points 1 to 4 (Figure 7). However, three values of τ_{bias} are required: 90 MPa for $\varepsilon^p_{global} < 0.5$ pct, 30 MPa for 0.5 pct $< \varepsilon^p_{global} <$ 1.5 pct, and 0 MPa for $\varepsilon^p_{global} > 1.5$ pct. The normal distribution is unable to produce a sufficient hysteretic width and reverse slip, even for large τ_{bias}. Finally, step 6 determines ε^p_{pre} = −0.4 pct as the best match to the initial yield and small strain monotonic $\sigma-\varepsilon$ behavior. This is generically consistent with experimental measurements of very inhomogeneous stress in ED NC Ni.[23] Overall, the best fitting parameters are summarized in Table III and include modest adjustments to the analytic estimates from steps 1 through 4, obtained by iteration based on repeated QCP simulations.

IV. PREDICTIONS OF THE CALIBRATED MODEL

A. *Fraction of Grains Undergoing Forward vs Reverse Slip*

The QCP simulations are capable of providing statistics on the nature of forward *vs* backward slip. Table IV shows the QCP simulation results, as calibrated to the ED NC (30 nm) Ni data in Figure 7. The predictions for reverse plastic strain ε^p_{rev} and the ratio $\varepsilon^p_{rev}/\varepsilon^p$ of reverse plastic strain to imposed plastic strain are within 10 pct of experimental values. A qualification is that the ε^p_{rev} values adopted from experimental data include the time-dependent relaxation strain obtained after unloading to 10 MPa and holding for 20 minutes.[10] In contrast, the ε^p_{rev} values from simulations are time independent and are simply the instantaneous values upon unloading to 0 MPa. The experimental data (and simulations) show that ε^p_{rev} increases to a peak of 0.28 pct and $\varepsilon^p_{rev}/\varepsilon^p$ decreases to a minimum of 13 pct as the stress σ_u at unload increases to $\sigma_{plateau}$. The simulations predict the fraction f_f of forward slipping grains to reach 87 pct at $\sigma_{plateau}$. Thus, there is a subset (13 pct) of grains that remain elastic even at large strain (ε^p = 2 pct). After unloading, the fraction f_b/f_f of backward-slipped to forward-slipped grains decreases from >60 pct at small ε^p to ~37 pct at large ε^p.

Table III. Best Fit of QCP Parameters to NC Ni (d_{mean} = 30 nm)

d	30 nm
τ_c	asymmetric distribution (Eq. [5a]) $\tau_{c,mean}$ = 1050 MPa, $\tau_{c,min}$ = 210 MPa
τ_{bias}	90 MPa, for $\varepsilon^p_{global} < 0.5$ pct 30 MPa, for 0.5 pct $< \varepsilon^p_{global} <$ 1.5 pct; 0 MPa, for $\varepsilon^p_{global} > 1.5$ pct
γ_{target}	$3.5 \cdot 10^{-3}$ to $1.0 \cdot 10^{-2}$ (Eq. [6])

Table IV. Plastic Recovery in NC Ni (d_{mean} = 30 nm)

		Model Fitted Results		Model Predicted Results		
	σ_u (MPa)	ε^p_{rev}	$\varepsilon^p_{rev}/\varepsilon^p$	f_f*	f_b**	f_b/f_f
1	800	0.0007	40 pct	33 pct	20 pct	62 pct
2	1100	0.0013	33 pct	45 pct	27 pct	60 pct
3	1400	0.0020	20 pct	70 pct	32 pct	45 pct
4	1600	0.0028	13 pct	87 pct	32 pct	37 pct

*f_f: fraction of slipped grains at $\sigma = \sigma_u$.
**f_b: fraction of backward slipped grains upon unloading.

B. *Characteristics of Grains with Backward Slip*

Grains with backward slip tend to have a relatively small τ_c and a relatively large number of forward slip events compared to their neighbors. Figure 8(a) shows the number of forward slip events q_f (Eq. [1]) in each grain at σ_{global} = 800 MPa (pt. 1', Figure 7). The plastically deformed grains are mainly isolated and surrounded by elastically deformed grains. Figure 8(b) shows the result upon unloading (pt. 1, Figure 7). During unloading, elastic-only grains attempt to return to their original dimension, driving 62 pct of plastically deformed grains to slip backward (Table IV). This leaves a small subset of grains with a nonzero q_f after unloading.

QCP simulations reveal the nature of grains that slip backward. Figure 8(c) displays the number of backward slip events q_b in grain i *vs* τ_c for grain i, for i = 1 to 1000 grains in the polycrystal, during unloading from ~800 MPa. The results show that backward slip tends to occur in grains with $\tau_c < 500$ MPa, and the number of backward slip events increases with decreasing τ_c. Figure 8(d) displays q_b *vs* the ratio $(q^n_f/q_f)_{800\ MPa}$ of forward slip events per neighboring grain (on average)

to forward slip events in grain i. The ratio is evaluated at $\sigma_{\text{global}} = 800$ MPa, just prior to unloading. The results show that the number of backward slip events tends to be larger in grains with a relatively large forward slip (*i.e.*, $q_f^n / q_f < 1$).

C. *Plastic Deformation and Residual Stress State*

Plastic deformation is capable of either reducing or enhancing the magnitude of residual stress. Figure 9 shows the predicted distribution of residual stress $\sigma_{z,\text{res}}$ at three unloaded states: just prior to tension testing, after unloading from $\sigma_{\text{global}} = 800$ MPa, and after unloading from $\sigma_{\text{global}} = 1400$ MPa. These correspond to states 0, 1, and 3 in Figure 7. The state 0 distribution (Figure 9(a)) is due to predeformation ($\varepsilon^p_{\text{pre}} = -0.4$ pct). The state 1 distribution is very sharp, indicating that the residual stress is dramatically reduced if the sample is stressed to 800 MPa and unloaded. This is achieved on a local grain scale by reversing slip events produced by predeformation. The state 3 distribution is very broad, indicating that the residual stress is dramatically increased if the sample is further stressed (to 1400 MPa) and unloaded. Such a large stress induces more slip events, beyond that needed to reverse the effects of predeformation.

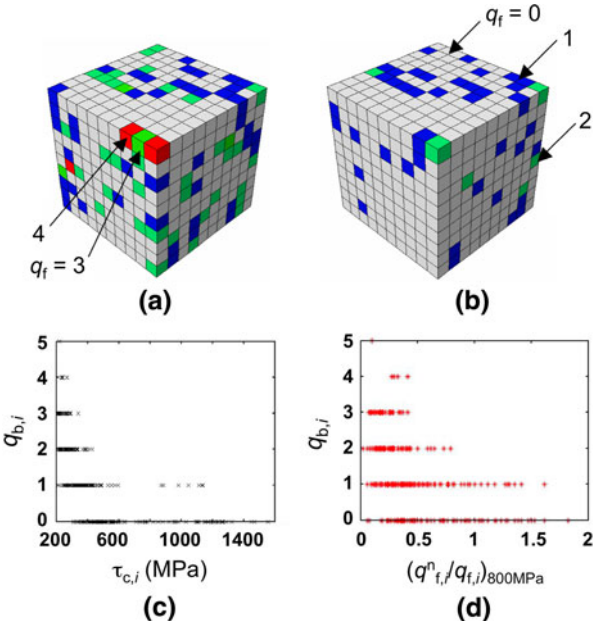

Fig. 8—Grain-to-grain distribution of the number of forward slip events q_f, obtained from QCP simulations for ED NC Ni with mean grain size $d_{\text{mean}} = 30$ nm (parameters in Table III) at (*a*) $\sigma_{\text{global}} = 800$ MPa (pt. 1′, Fig. 7) and (*b*) after unloading to $\sigma_{\text{global}} = 0$ MPa (pt. 1, Fig. 7). (*c*) Number of backward slip events $q_{b,i}$ in grain i during unloading from pts. 1′ to 1, *vs* the critical resolved shear stress $\tau_{c,i}$ in grain i. (*d*) $q_{b,i}$ *vs* the ratio $(q^n_{f,i}/q_{f,i})_{800\text{ MPa}}$ of the average number of forward slip events in grains that border grain i to the number of forward events in grain i. The ratio is evaluated at $\sigma_{\text{global}} = 800$ MPa (pt. 1′, Fig. 7).

V. SUMMARY AND CONCLUSIONS

A QCP constitutive relation is implemented in a finite element model to study the monotonic and cyclic response of NC metals. Key model parameters include the grain-to-grain distribution (τ_c) of critical strength to activate slip events, a bias in the critical strength to active forward *vs* backward slip (τ_{bias}), and the amount of plastic pre-deformation ($\varepsilon^p_{\text{pre}}$). A principal outcome is a six-step process (Table II) by which to extract these quantities from experimental measurements of monotonic and cyclic $\sigma-\varepsilon$ response. This process is applied to data for ED Ni with a 30-nm mean grain size. Several observations are made.

1. Plastic pre-deformation ($\varepsilon^p_{\text{pre}}$) induces a residual stress state that enhances or suppresses slip events during subsequent loading. This creates an *effective* distribution of critical strengths (τ_c^{eff}) that can increase or decrease the macrostress for yield and make the elastoplastic transition abrupt or extended.
2. Similar τ_c^{eff} distributions and thus similar monotonic responses can be achieved by more than one combination of (τ_c, $\varepsilon^p_{\text{pre}}$). Thus, τ_c and $\varepsilon^p_{\text{pre}}$ cannot be uniquely determined from monotonic $\sigma-\varepsilon$ data alone.
3. A less redundant determination of τ_c, $\varepsilon^p_{\text{pre}}$, and τ_{bias} can be made by fitting the QCP predictions to monotonic *and* cyclic $\sigma-\varepsilon$ at small *and* large strain.
4. The best fit for ED Ni ($d_{\text{mean}} = 30$ nm) has a truncated (asymmetric) τ_c distribution, $\varepsilon^p_{\text{pre}} = -0.4$ pct, and $\tau_{\text{bias}} = 90$ MPa at small strain and 0 MPa at large strain. The asymmetric distribution is consistent with an abrupt onset of slip in a large fraction

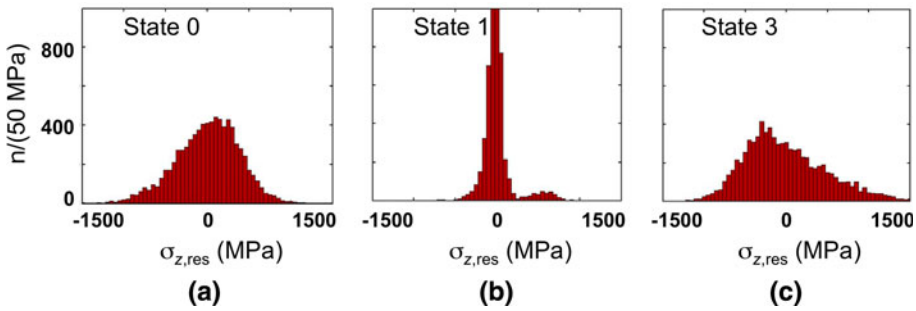

Fig. 9—Distribution of residual stress $\sigma_{z,\text{res}}$ at different states in Fig. 7: (*a*) initial state 0, prior to loading; (*b*) state 1, after unloading from $\sigma_{\text{global}} = 800$ MPa; and (*c*) state 3, after unloading from $\sigma_{\text{global}} = 1400$ MPa.

of grains at a critical resolved shear stress ~1/grain size. The bias is consistent with backward slip requiring a smaller mechanical driving force (stress) than forward slip.
5. The simulations capture the large reversible deformation observed in experiments and predict reverse slip to occur in relatively soft grains having smaller τ_c and more slip events than their neighbors.
6. The QCP simulations predict that quantized slip often induces very inhomogeneous stress states. These inhomogeneous states store large elastic energy that can drive reversible deformation.
7. The QCP simulations also show that inhomogeneous stress induced by prior deformation can be reduced, in principle, *via* subsequent deformation.
8. Despite the capacity of the QCP simulations to capture monotonic and cyclic $\sigma-\varepsilon$ data, there are important qualifications. First, the distribution of critical strengths (τ_c) is quite simple. It does not evolve with deformation and all slip systems within a grain are assumed to have the same τ_c. In reality, the nature of grain boundaries (and thus τ_c) is expected to evolve with deformation. This is reflected, in part, by a fitted value of τ_{bias} that evolves from 90 MPa at small strain to 0 MPa at large strain. Second, one cubic element is employed to represent each grain so that specific grain geometries, constraints from neighboring grains, and stress concentrations from localized slip are captured in a grain-average sense. Third, only the largest slip events are modeled in these simulations, leaving out numerous smaller events associated with slip across corners or smaller cross sections of grains. Fourth, there is no explicit time or temperature dependence to the slip processes. Finally, there is no explicit modeling of grain boundary sliding or grain growth during deformation. Despite these deficiencies, the QCP simulations capture a unique characteristic of plastic deformation observed in MD simulations, allowing NC deformation to be studied at length and time scales not accessible to MD simulations.

ACKNOWLEDGMENTS

Two of the authors (LL and PMA) thank Helena Van Swygenhoven and Steven Van Petegem, Paul Scherrer Institute, for the experimental data (d_{mean} = 30 nm) and for helpful discussions. Support from the United States National Science Foundation (Grant No. DMR0907024), the International Centre for Materials Research (Grant No. DMR04-09848), and the Ohio Supercomputer Center (Grant No. PAS0676-5) are greatly appreciated.

REFERENCES

1. L. Li, P.M. Anderson, M.G. Lee, E. Bitzek, P. Derlet, and H. Van Swygenhoven: *Acta Mater.*, 2009, vol. 57, pp. 812–22.
2. E. Bitzek, P.M. Derlet, P. Anderson, and H. Van Swygenhoven: *Acta Mater.*, 2008, vol. 56, pp. 4846–57.
3. K.S. Kumar, H. Van Swygenhoven, and S. Suresh: *Acta Mater.*, 2003, vol. 51, pp. 5743–74.
4. M.A. Meyers, A. Mishra, and D.J. Benson: *Prog. Mater. Sci.*, 2006, vol. 51, pp. 427–556.
5. J. Rajagopalan, J.H. Han, and M.T.A. Saif: *Science*, 2007, vol. 315, pp. 1831–34.
6. J. Rajagopalan, J.H. Han, and M.T.A. Saif: *Scripta Mater.*, 2008, vol. 59, pp. 734–37.
7. I. Lonardelli, J. Almer, G. Ischia, C. Menapace, and A. Molinari: *Scripta Mater.*, 2009, vol. 60, pp. 520–23.
8. Z. Budrovic, H. Van Swygenhoven, P.M. Derlet, S. Van Petegem, and B. Schmitt: *Science*, 2004, vol. 304, pp. 273–76.
9. S. Brandstetter, Z. Budrovic, S. Van Petegem, B. Schmitt, E. Stergar, P.M. Derlet, and H. Van Swygenhoven: *Appl. Phys. Lett.*, 2005, vol. 87, pp. 231910-1–2.
10. S. Brandstetter, H. Van Swygenhoven, S. Van Petegem, B. Schmitt, R. Maass, and P.M. Derlet: *Adv. Mater.*, 2006, vol. 18, pp. 1545–48.
11. S. Van Petegem, S. Brandstetter, H. Van Swygenhoven, and J.L. Martin: *Appl. Phys. Lett.*, 2006, vol. 89, pp. 073102-1–3.
12. H. Van Swygenhoven: *Nat. Mater.*, 2006, vol. 5, pp. 841–41.
13. H. Van Swygenhoven, P.M. Derlet, and A.G. Froseth: *Nat. Mater.*, 2004, vol. 3, pp. 399–403.
14. H. Van Swygenhoven, P.M. Derlet, and A.G. Froseth: *Acta Mater.*, 2006, vol. 54, pp. 1975–83.
15. H. Van Swygenhoven, P.M. Derlet, and A. Hasnaoui: *Phys. Rev. B*, 2002, vol. 66, pp. 024101-1–8.
16. V. Yamakov, D. Wolf, S.R. Phillpot, A.K. Mukherjee, and H. Gleiter: *Nat. Mater.*, 2004, vol. 3, pp. 43–47.
17. ABAQUS, *ABAQUS Reference Manuals*, Hibbitt, Karlsson & Sorensen Inc., Pawtucket, RI, 2005.
18. S.R. Kalidindi, C.A. Bronkhorst, and L. Anand: *J. Mech. Phys. Solids*, 1992, vol. 40, pp. 537–69.
19. H.B. Huntington: *Solid State Phys.*, 1958, vol. 7, p. 213.
20. *Ohio Supercomputer Center*, http://www.osc.edu/supercomputing/computing/opt/index.shtml.
21. F. Ebrahimi, G.R. Bourne, M.S. Kelly, and T.E. Matthews: *Nanostruct. Mater.*, 1999, vol. 11, pp. 343–50.
22. M. Zaiser and N. Nikitas: *J. Stat. Mech. Theory Exp.*, 2007, vol. 2007, pp. P04013-1–10.
23. A.M. El-Sherik, J. Shirokoff, and U. Erb: *J. Alloys Compd.*, 2005, vol. 389, pp. 140–43.